PAPER

Shape-controlled synthesis of magnetic Fe_3O_4 nanoparticles with different iron precursors and capping agents

Hira Fatima, Dae-Won Lee, Hyun Joong Yun and Kyo-Seon Kim [iD] *

This paper describes a modified method to prepare monodisperse Fe_3O_4 magnetic nanoparticles with different shapes (cube, octahedron, and sphere). The shape of the magnetic nanoparticles could be conveniently controlled by changing the types of precursor/capping agent and concentration of capping agent. The prepared samples were characterized using scanning electron microscopy, X-ray diffraction and vibrating sample magnetometry. Cubes and octahedra were formed using ferrous sulfate heptahydrate as an iron source, ethylene glycol as a solvent and potassium hydroxide (KOH) as a capping agent while spheres were formed by using ferric chloride hexahydrate as an iron source, ethylene glycol as a solvent and ammonium acetate as a capping agent. By varying KOH concentration (0.5 M, 1 M, 1.5 M, and 5 M), the shape was transformed from cubes to octahedra because octahedra are developed dominantly at higher concentration of KOH within the reaction mixture. The magnetic studies show superparamagnetic behavior for all samples at room temperature. The Fe_3O_4 nanoparticles show the magnetic saturation values of 87 emu g^{-1}, 85 emu g^{-1}, and 82 emu g^{-1} for spheres, cubes, and octahedrons, respectively.

Introduction

Magnetic nanoparticles (MNPs) have been attracting much attention because of their prospective applications either as a separator in bioseparation of proteins, DNA, *etc.*,[1] contrast agent in magnetic resonance imaging,[2] heating mediator for magnetic hyperthermia,[3] sensor for the detection of urea[4] and glucose,[5] transport agent in gene delivery[6] and drug delivery, and cell sorting.[7] Particularly, iron oxide (Fe_3O_4) nanoparticles have attracted considerable interest, because of their biocompatibility, unique magnetic properties, high electrical resistivity and high chemical stability.[8,9] It is commonly known that the activity of Fe_3O_4 MNPs strongly depends on their size, shape and crystal phase.[10,11] Notably, the shape has a great impact on the resulting properties of Fe_3O_4 MNPs and their potential applications. Indeed, changing the crystal shape of Fe_3O_4 MNPs alters the exposed crystal facets and hence the atomic arrangements in each facet, which will have significant impacts on their various properties.[12]

The interesting potential applications of Fe_3O_4 MNPs have encouraged the rapid development of several synthetic techniques such as coprecipitation,[13,14] hydrothermal treatment,[15] spray pyrolysis,[16] ultrasound irradiation,[17] microwave-assisted method[18,19] and solvothermal method.[20] Recently, a variety of novel shapes such as nanorods,[21] nanowires[21] and nanosheets[22]

have been reported. It still remains challenging for the material scientist to control the shape of Fe_3O_4 MNPs by controlling the type/concentration of reactant, type of surfactant and reaction temperature.

Herein, we demonstrate that, under appropriate experimental conditions, uniform spinel nanostructures of cube, octahedron, and sphere can be successfully synthesized *via* a facile, safe and convenient method. Depending on the iron source and type of surfactant, different shapes of Fe_3O_4 MNPs were prepared. The magnetic properties are also compared for different shapes of Fe_3O_4 nanoparticles.

Experimental section

All the chemicals in this study were commercially available and of analytical grade, including ferrous sulfate heptahydrate ($FeSO_4 \cdot 7H_2O$, $\geq 98\%$) and ferric chloride hexahydrate ($FeCl_3 \cdot 6H_2O$, $\geq 98\%$), ammonium acetate (NH_4Ac, $\geq 98\%$), potassium hydroxide (KOH), ethylene glycol (EG), ethanol and concentrated hydrochloric acid (HCl, 36.5%).
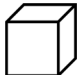
Synthesis of Fe_3O_4 MNPs by using an iron precursor of $FeSO_4 \cdot 7H_2O$

0.2780 g of the $FeSO_4 \cdot 7H_2O$ was dissolved in 5 mL of EG to form a homogeneous solution. Then, the controlled amount of KOH solution (0.5 M, 1 M 1.5 M or 5 M) was added to the prepared iron salt solution at room temperature under

Department of Chemical Engineering, Kangwon National University, Chuncheon, Kangwon-Do, 200-701, Korea. E-mail: kkyoseon@kangwon.ac.kr

Table 1 Synthesis conditions to prepare Fe$_3$O$_4$ MNPs with various morphologies

	Sphere (S)	Cube (C)	Transformation undergoing	Transformation undergoing	Octahedron (O)
Morphologies of product			C → O	C → O	
Iron precursor	FeCl$_3$·6H$_2$O	FeSO$_4$·7H$_2$O	FeSO$_4$·7H$_2$O	FeSO$_4$·7H$_2$O	FeSO$_4$·7H$_2$O
NH$_4$Ac	1 M	—	—	—	—
KOH quantity (mol L^{-1})	—	0.5 M	1 M	1.5 M	5 M
Solvent	EG	EG	EG	EG	EG
Size	216.6 nm	158.5 nm	160 nm	581.2 nm	4.9 μm

stirring. The mixture stirring was continued to get a homogeneous solution. The resultant homogeneous mixture solution was then transferred to a 30 mL Teflon lined stainless steel autoclave, was sealed and maintained at 200 °C for 24 h. After the completion of the reaction, the black solid products were collected by magnetic separation and washed with ethanol three times. The final products were dried in a vacuum oven at 40 °C for 6 h.

Synthesis of Fe$_3$O$_4$ MNPs by using an iron precursor of FeCl$_3$·6H$_2$O

Typically, a solution of EG containing 0.1 M FeCl$_3$·6H$_2$O (Sigma-Aldrich, ≥98%) and 1 M of NH$_4$Ac (Sigma, ≥98%) was made and well mixed for 7 h. The solution mixture was then transferred to a Teflon-lined autoclave cell, was sealed and maintained at 200 °C for 24 h. The autoclave cell was allowed to cool down quickly to room temperature by spraying tap water on it. The synthesized particles were separated by a magnet and washed with ethanol and water, respectively, three times and then were dried in a vacuum oven at 60 °C for 6 h before characterization.

Characterization of Fe$_3$O$_4$ MNPs prepared

The scanning electron microscopy (SEM) measurements of surface and cross-section of the product particles were carried out with a Hitachi S-4800 ultra-high resolution SEM equipment using a 15 kV electron beam with the resolution of 1 nm. Powder X-ray diffraction (XRD) patterns were recorded with a Philips X'Pert PRO MPD X-ray diffractometer using Cu Kα radiation (k51.54060 A°, 40 kV, 30 mA). The samples were scanned in step of 0.017° in the 2θ range of 20–80°. The magnetic properties of product particles were also measured with a Lake Shore £7300 vibrating sample magnetometer (VSM).

Results and discussion

The different synthetic conditions of Fe$_3$O$_4$ MNPs are described in Table 1. The morphologies of the as-synthesized products were investigated by SEM. The Fe$_3$O$_4$ MNPs with the shapes of cube, octahedron and their mixtures were formed,

when FeSO$_4$·6H$_2$O was used as the iron source with various KOH concentrations (0.5 M, 1 M 1.5 M, and 5 M). It is shown that the type of precursor and concentration of surfactant are critically important for controlling the shape of nanoparticles without the need of shape sorting or seeding processes. The nanoparticle shape was invariably cubic (see Fig. 1a and b), when 0.5 M KOH concentration was added.

The main driving force for the transformation from cubic to octahedron is the change in KOH concentration and the increase in OH^{1-} concentration favors the formation of the octahedron. For the increase in KOH concentration to 1 M, the shape transformation from cube to octahedron was observed with an average particle diameter ranging from 200–300 nm. The formation of octahedron may be attributed to the continued growth along the corners of cubic shape as shown in Fig. 1c and d. Further increase in KOH concentration to 1.5 M resulted in the unsymmetrical octahedron. Small cubes were also present with irregular boundaries (Fig. 1e and f). Higher concentration of KOH in the reaction mixture provides the higher concentration of OH^{1-} ions to generate higher chemical potential within the solution, which is the favorable condition for the formation of octahedral structures (Fig. 1g and h).[23]

One more study also confirms that the increase in KOH concentration favors the crystal growth along [111] plane which helps develop octahedral structures.[24] The shape of the nanocrystal is mostly dependent on the growth rate along different planes. Wang et al.[24] suggested that the shape of Fe$_3$O$_4$ MNPs face-centered cubic (fcc) structure varies with the ratio of two different growth planes i.e. [100] and [111]. Their results demonstrate that higher concentration of KOH during synthesis favors the faster growth rate along [111] plane than that of [100] plane. Swaminathan et al.[25] also studied the impact of crystal growth rates along different planes on the shape of nanoparticles. The faster crystal growth along [111] plane develops octahedral structures, while the cubes are formed due to the faster growth along [100] plane. The experimental yield of Fe$_3$O$_4$ MNPs obtained in this study is about 80.5%. There are two main causes of yield loss. Firstly, some particles are lost during the magnetic separation and washing. Especially, smaller sized particles have the higher chances to be lost due to their low magnetic strength.
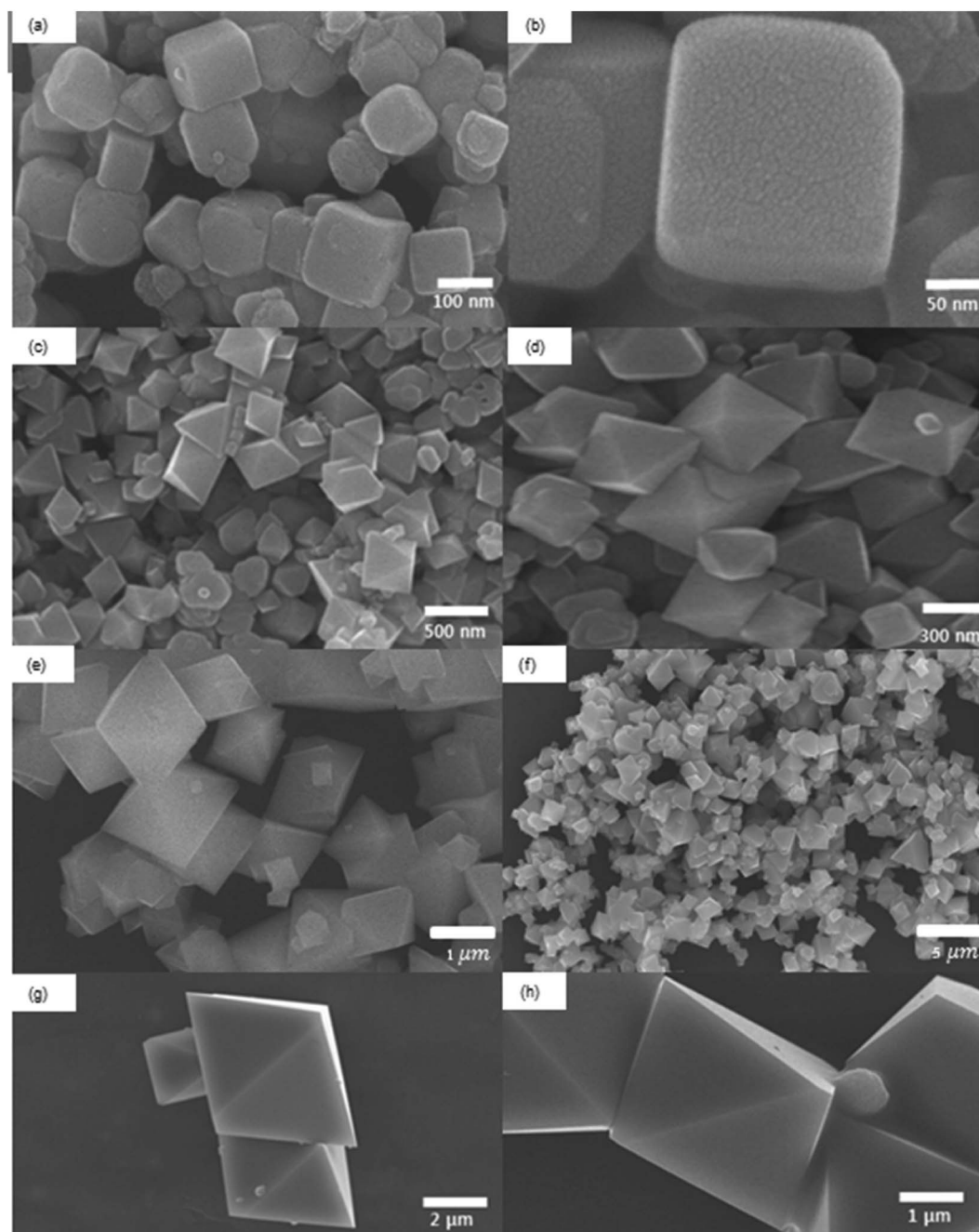
Fig. 1 SEM images of Fe_3O_4 MNPs for different KOH concentrations using iron precursor of $FeSO_4 \cdot 7H_2O$. (a and b) 0.5 M, (c and d) 1 M, (e and f) 1.5 M and (g and h) 5 M.

Secondly, some particles can be lost during ultrasonic cleaning, because some droplets are generated and lost during this process. We can increase the collection yield by reducing the number of washing and also designing more carefully the magnetic separation and washing.

The crystal structures of the samples were also studied by XRD. The intensities and positions of diffraction peaks of the cube (Fig. 2a) and octahedron (Fig. 2b) match with those of Fe_3O_4 MNPs in the literature.[26] The diffraction peaks at $2\theta = 44°$ assign to the fcc structure of Fe_3O_4 nanoparticles. For both samples, X-ray diffraction peaks corresponding to Bragg diffractions of the crystal planes of (111), (220), (311), (222), (400), (422) and (511) agree with standard JCPDS patterns, which indicates the high crystal phase purity of synthesized Fe_3O_4, (from Pdf reference code, Fig. 2a = 01-086-1344 and Fig. 2b = 01-089-0688).[2,6] Moreover, the (111) facet becomes stronger at $2\theta = 18$ as the morphology of Fe_3O_4 MNPs transfers from cubic to octahedron which is consistent with the literature reported.[27]
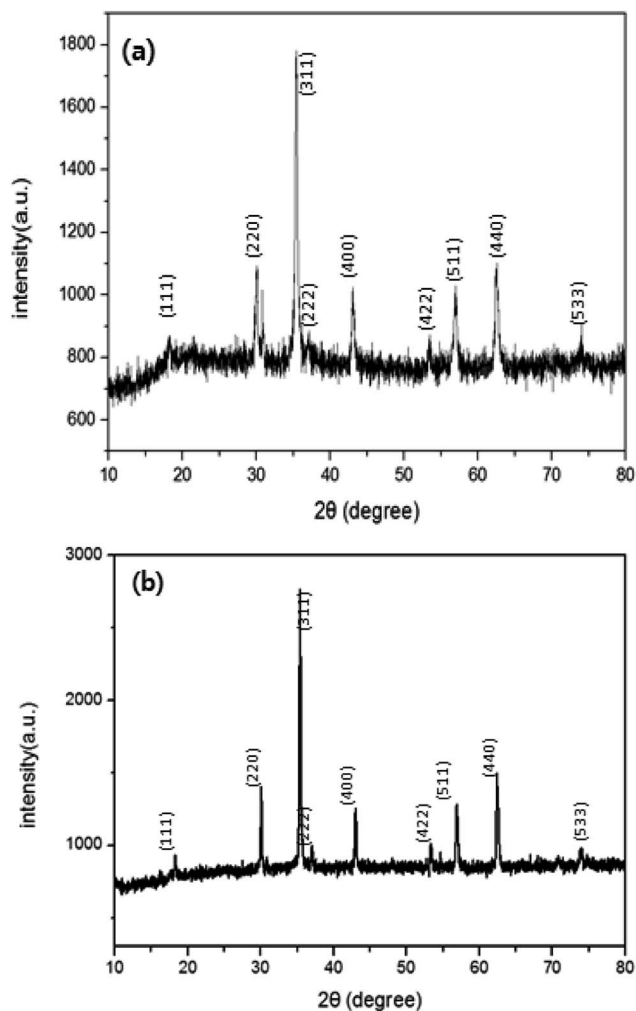
Fig. 2 XRD patterns of Fe$_3$O$_4$ MNPs derived from different concentrations of KOH, using iron precursor of FeSO$_4$·7H$_2$O. (a) 0.5 M (cube) and (b) 5 M of KOH concentration (octahedron).

Fig. 3 (a and b) SEM images of Fe$_3$O$_4$ MNPs using iron precursor of FeCl$_3$·6 H$_2$O (spheres).

Spherical Fe$_3$O$_4$ MNPs with an average particle size of 200–300 nm were formed by using FeCl$_3$.6H$_2$O iron precursor as shown in Fig. 3. The spheres formed in Fig. 3a shows the uniform morphology and narrow size distribution and are vital to gain the maximum susceptibility at low magnetic field.[28] Magnified SEM images show that spherical nanoparticles are composed of many smaller grains (Fig. 3b). X-ray diffraction patterns were recorded to determine the phase purity of Fe$_3$O$_4$ spherical nanoparticles (Fig. 4). X-ray diffraction peaks corresponding to Bragg diffractions of the crystal planes of (220), (311), (222), (400), (422), (511) and (440) agree with standard JCPDS patterns, which indicates high crystal phase purity of synthesized Fe$_3$O$_4$ spherical nanoparticles. The diffraction peaks show the fcc structure of spherical Fe$_3$O$_4$ nanoparticles with high crystallinity.

The magnetic properties of Fe$_3$O$_4$ nanoparticles of different shapes were studied with a VSM at room temperature. Fig. 5 shows the magnetic hysteresis curves measured for the samples synthesized. Magnetization hysteresis wa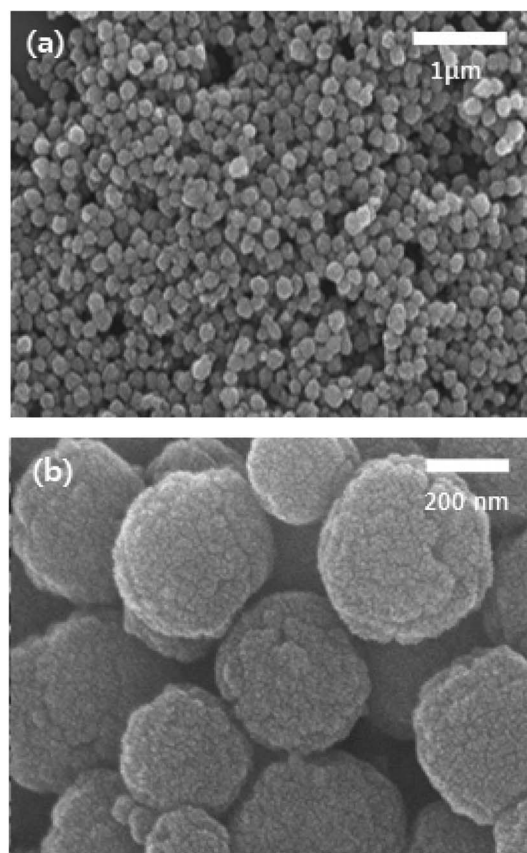s close to zero for all samples and this is common for superparamagnetic iron oxide nanoparticles and confirms their superparamagnetic nature of Fe$_3$O$_4$ nanoparticles prepared in this study.[29] The magnetic saturation values of 87 emu g^{-1}, 85 emu g^{-1}, and 82 emu g^{-1} were observed for Fe$_3$O$_4$ nanoparticles with the shapes of spheres (216.6 nm), cubes (158.5 nm), and octahedral (4.9 μm), respectively. The saturation magnetization values were found to be higher than those of Fe$_3$O$_4$ nanowires (71 emu g^{-1}),[30] nanopyramid (52.5 emu g^{-1}),[31] 40 emu g^{-1} nanocubes[29] and 31 emu g^{-1} nanospheres[29] in the literature.

In principle, shape anisotropy alters the magnetic saturation values of nanostructures.[31] The high symmetry of Fe$_3$O$_4$ MNPs will lead to low shape anisotropy, which is one reason for the spherical sample to have higher magnetization values relative to the cubes or octahedron. Zhao *et al.* reported the shape anisotropy of different shaped nanoparticles as follows; spheres < cubes < transformed particles < octahedron.[23] The symmetrical particles show high magnetization values and are easier to magnetize along the long direction than along the short directions,[32] which will help to release more heat even at low concentration during hyperthermia heating. The unsymmetrical shape results in the breaking of the local symmetry of nanoparticles which breaks the symmetry bond and cause surface strain,[33] which will eventually reduce the magnetization values.
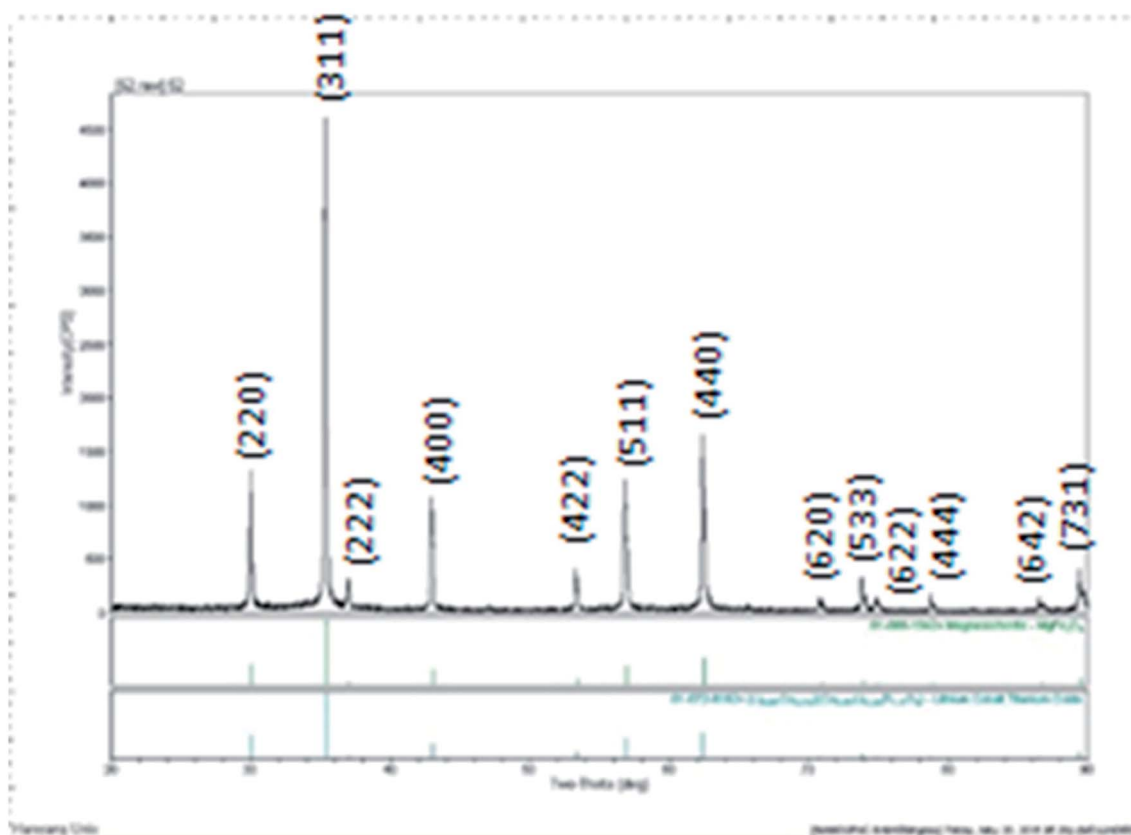
Fig. 4 XRD pattern of Fe$_3$O$_4$ MNPs using iron precursor of FeCl$_3\cdot$6 H$_2$O (spheres).

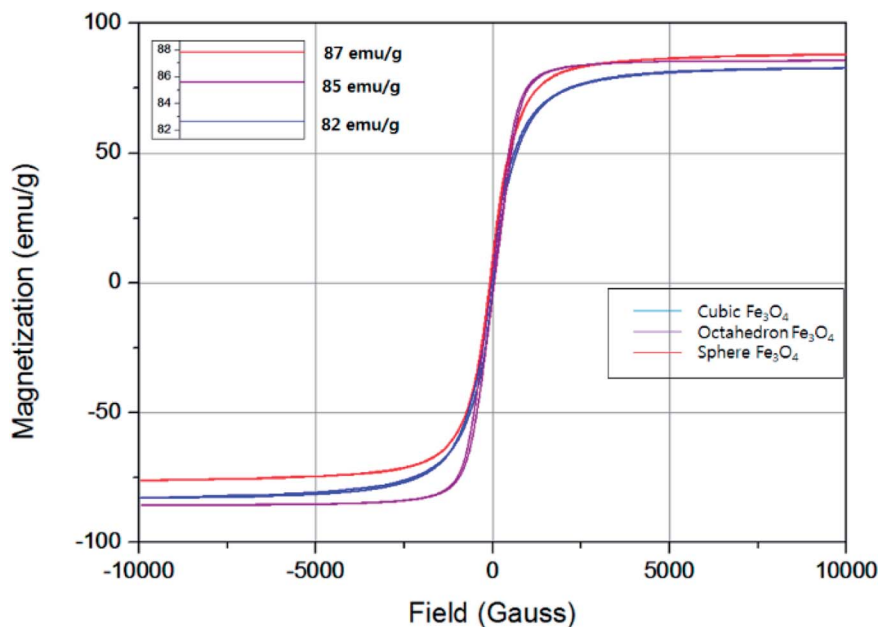**Fig. 5** VSM profile of Fe$_3$O$_4$ nanoparticles of different shapes using iron precursors of FeSO$_4\cdot$7H$_2$O (cubes & octahedron) and of FeCl$_3\cdot$6 H$_2$O (spheres).

Conclusion

We synthesized the Fe$_3$O$_4$ magnetic nanostructures of different shapes by changing the types of precursor/capping agent and concentration of capping agent. A modified method to prepare monodisperse Fe$_3$O$_4$ magnetic nanoparticles with different shapes (cube, octahedron, and sphere) has been presented using an autoclave system in the presence of KOH/NH$_4$Ac as

a capping agent. Cubes and octahedron were formed using $FeSO_4 \cdot 7H_2O$ as an iron precursor and KOH as a capping agent while spheres were formed by using $FeCl_3 \cdot 6H_2O$ as an iron source and NH_4Ac as a capping agent. By varying KOH concentration (0.5 M, 1 M, 1.5 M, and 5 M), the shape was transformed from cube to octahedron that is due to the presence of higher number of OH^{1-} ions within the reaction mixture which favors the formation of the octahedron. Moreover, a higher concentration of KOH also favors the faster growth rate along [111] plane than that of [100] plane. The prepared Fe_3O_4 magnetic nanoparticles have the fcc structure and the particle sizes are about 200–300 nm. The Fe_3O_4 nanoparticles show the superparamagnetic properties and have the magnetic saturation values of 87 emu g^{-1}, 85 emu g^{-1}, and 82 emu g^{-1} for spheres, cubes, and octahedrons, respectively.

Conflicts of interest

There are no conflicts of interest.

Acknowledgements

References

1 H. Fatima and K.-S. Kim, Magnetic nanoparticles for bioseparation, *Korean J. Chem. Eng.*, 2017, **34**(3), 589–599.

2 N. Naseer, *et al.*, Magnetically responsive hybrid polymer colloids for ultrasensitive molecular imaging, *J. Colloid Sci. Biotechnol.*, 2014, **3**(1), 19–29.

3 S. Laurent, *et al.*, Magnetic fluid hyperthermia: focus on superparamagnetic iron oxide nanoparticles, *Adv. Colloid Interface Sci.*, 2011, **166**(1–2), 8–23.

4 A. Zaibudeen and J. Philip, Magnetic nanofluid based non-enzymatic sensor for urea detection, *Sens. Actuators, B*, 2018, **255**, 720–728.

5 V. Mahendran and J. Philip, Non-enzymatic glucose detection using magnetic nanoemulsions, *Appl. Phys. Lett.*, 2014, **105**(12), 123110–123114.

6 S. I. Stoeva, *et al.*, Three-layer composite magnetic nanoparticle probes for DNA, *J. Am. Chem. Soc.*, 2005, **127**(44), 15362–15363.

7 T. Neuberger, *et al.*, Superparamagnetic nanoparticles for biomedical applications: possibilities and limitations of a new drug delivery system, *J. Magn. Magn. Mater.*, 2005, **293**(1), 483–496.

8 W. Wu, C. Jiang and V. A. Roy, Recent progress in magnetic iron oxide–semiconductor composite nanomaterials as promising photocatalysts, *Nanoscale*, 2015, **7**(1), 38–58.

9 J. Y. Park, S. G. Oh and B. H. Ha, Characterization of iron (III) oxide nanoparticles prepared by using ammonium acetate as precipitating agent, *Korean J. Chem. Eng.*, 2001, **18**(2), 215–219.

10 Q. Huang, L. Zou and D. Chen, Phase and morphology controlled in the synthesis of iron oxide particles: dimension-based carbonaceous materials as modifiers, *RSC Adv.*, 2016, **6**(85), 82294–82297.

11 K.-S. Kim, Functionalization of magnetic nanoparticles for biomedical applications, *Korean J. Chem. Eng.*, 2014, **31**(8), 1289–1305.

12 Y. Eom, *et al.*, Morphology-controlled synthesis of highly crystalline Fe_3O_4 and $CoFe_2O_4$ nanoparticles using a facile thermal decomposition method, *RSC Adv.*, 2016, **6**(19), 15861–15867.

13 P. L. Hariani, M. Faizal and D. Setiabudidaya, Synthesis and properties of Fe_3O_4 nanoparticles by co-precipitation method to removal procion dye, *Int. J. Environ. Sci. Dev.*, 2013, **4**(3), 336–351.

14 T. Muthukumaran and J. Philip, Effect of phosphate and oleic acid capping on structure, magnetic properties and thermal stability of iron oxide nanoparticles, *J. Alloys Compd.*, 2016, **689**, 959–968.

15 Y. Khollam, *et al.*, Microwave hydrothermal preparation of submicron-sized spherical magnetite (Fe_3O_4) powders, *Mater. Lett.*, 2002, **56**(4), 571–577.

16 C. Wang, *et al.*, The preparation of magnetite Fe_3O_4 and its morphology control by a novel arc-electrodeposition method, *Mater. Res. Bull.*, 2002, **37**(15), 2525–2529.

17 R. V. Kumar, *et al.*, Fabrication of magnetite nanorods by ultrasound irradiation, *J. Appl. Phys*, 2001, **89**(11), 6324–6328.

18 W.-W. Wang, Y.-J. Zhu and M.-L. Ruan, Microwave-assisted synthesis and magnetic property of magnetite and hematite nanoparticles, *J. Nanopart. Res.*, 2007, **9**(3), 419–426.

19 S. Kalyani, J. Sangeetha and J. Philip, Effect of Precipitating Agent and Solvent Polarity on the Size and Magnetic Properties of Magnetite Nanoparticles Prepared by Microwave Assisted Synthesis, *J. Nanosci. Nanotechnol.*, 2016, **16**(9), 9591–9602.

20 S.-B. Cho, *et al.*, Morphological control of Fe_3O_4 particles *via* glycothermal process, *J. Mater. Sci.*, 2007, **42**(13), 4877–4886.

21 H. Jiao and H. Yang, Thermal oxide synthesis and characterization of Fe_3O_4 nanorods and Fe_2O_3 nanowires, *Sci. China, Ser. B: Chem.*, 2009, **52**(5), 599–604.

22 K. C. Chin, *et al.*, Large-scale synthesis of Fe_3O_4 nanosheets at low temperature, *J. Phys. Chem. C*, 2007, **111**(26), 9136–9141.

23 L. Zhao, *et al.*, Morphology-controlled synthesis of magnetites with nanoporous structures and excellent magnetic properties, *Chem. Mater.*, 2007, **20**(1), 198–204.

24 Z. Wang, Transmission electron microscopy of shape-controlled nanocrystals and their assemblies, *J. Phys. Chem. B*, 2000, **104**(6), 1153–1175.

25 R. Swaminathan, M. Willard and M. McHenry, Experimental observations and nucleation and growth theory of polyhedral magnetic ferrite nanoparticles synthesized using an RF plasma torch, *Acta Mater.*, 2006, **54**(3), 807–816.

26 Q. Wang, *et al.*, Controllable synthesis and magnetic property of Fe/Fe_3O_4 polyhedron synthesized by

solvothermal method, *J. Mater. Sci.: Mater. Electron.*, 2012, **23**(8), 1527–1532.

27 B. Bateer, *et al.*, Facile synthesis and shape control of Fe_3O_4 nanocrystals with good dispersion and stabilization, *CrystEngComm*, 2013, **15**(17), 3366–3371.

28 E. Moreno, *et al.*, Preparation of narrow size distribution superparamagnetic γ-Fe_2O_3 nanoparticles in a sol–gel transparent SiO_2 matrix, *Langmuir*, 2002, **18**(12), 4972–4978.

29 G. Zhen, *et al.*, Comparative study of the magnetic behavior of spherical and cubic superparamagnetic iron oxide nanoparticles, *J. Phys. Chem. C*, 2010, **115**(2), 327–334.

30 J. Wang, *et al.*, Magnetic-Field-Induced Growth of Single-Crystalline Fe_3O_4 Nanowires, *Adv. Mater.*, 2004, **16**(2), 137–140.

31 F. Liu, *et al.*, Novel nanopyramid arrays of magnetite, *Adv. Mater.*, 2005, **17**(15), 1893–1897.

32 B. Issa, *et al.*, Magnetic nanoparticles: surface effects and properties related to biomedicine applications, *Int. J. Mol. Sci.*, 2013, **14**(11), 21266–21305.

33 E. C. Abenojar, *et al.*, Structural effects on the magnetic hyperthermia properties of iron oxide nanoparticles, *Prog. Nat. Sci.: Mater. Int.*, 2016, **26**(5), 440–448.